Carbon Nanotube Nanoelectromechanical Systems as Magnetometers for Single-Molecule Magnets

Marc Ganzhorn,[†] Svetlana Klyatskaya,[‡] Mario Ruben,[‡,§] and Wolfgang Wernsdorfer[†,*]

[†]Institut Néel, CNRS & Université Joseph Fourier, BP 166, 25 Avenue des Martyrs, 38042 Grenoble Cedex 9, France, [‡]Institut of Nanotechnology (INT), Karlsruhe Institute of Technology (KIT), 76344 Eggenstein-Leopoldshafen, Germany, and [§]IPCMS, Université de Strasbourg, 67034 Strasbourg, France

ABSTRACT Due to outstanding mechanical and electronic properties, carbon nanotube nanoelectromechanical systems (NEMS) were recently proposed as ultrasensitive magnetometers for single-molecule magnets (SMM). In this article, we describe a noninvasive grafting of a SMM on a carbon nanotube NEMS, which conserves both the mechanical properties of the carbon nanotube NEMS and the magnetic properties of the SMM. We will demonstrate that the nonlinearity of a carbon nanotube's mechanical motion can be used to probe the reversal of a molecular spin, associated with a bis(phthalocyaninato)terbium(III) single-molecule magnet, providing an experimental evidence for the detection of a single spin by a mechanical degree of freedom on a molecular level.

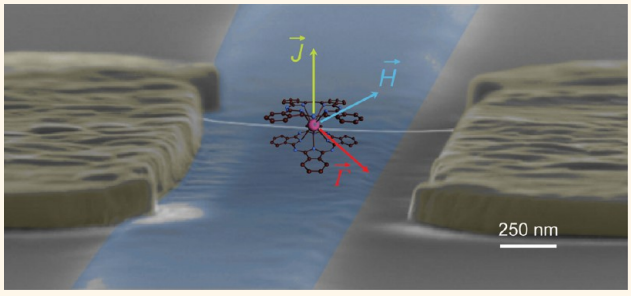

KEYWORDS: carbon nanotube · NEMS · magnetometer · single-molecule magnets

A single-molecule magnet (SMM) consists of magnetic centers, typically transition metal ions, embedded in a shell of organic ligands.[1,2] The ligands are designed to ensure the bonding of the molecule to surfaces or junctions while preserving and enhancing the ions' magnetic properties. The magnetic centers will therefore behave as a single "giant" spin due a strong interaction promoted by the ligands.[1] Moreover, one can replace the magnetic centers and therefore alter the magnetic properties of the compound without affecting the ligand shell and the interaction with its environment.[1,3] One can also modify the organic ligands by chemical engineering in order to change the SMM's coupling to its environment[1,2] or promote the selective grafting to a certain material, for example, carbon nanotubes or graphene.[4,5] Eventually, chemical engineering allows the synthesis of billions of perfectly identical molecules and would enable the high density integration of molecular spintronic devices.[1,2]

Provided with a large spin ground state combined with a strong uniaxial magnetic anisotropy, SMMs exhibit a wide range of quantum mechanical phenonoma such as quantum tunneling of magnetization[6,7] or quantum phase interference.[8] However, probing the quantum mechanical nature of an individual SMM still remains a considerable challenge.

Various detector designs for individual single-molecule magnets (SMMs) were consequently proposed over the past decade.[1] One can use for instance a scanning tunneling microscope to probe an isolated SMM on a conducting surface.[9−12] Alternatively, one can build a three-terminal molecular spin transistor where an individual SMM is bridging the gap between two nonmagnetic leads.[13,14] In such a configuration, the electric current is flowing directly through the molecule, leading to a strong coupling between the electrons and the magnetic core. This direct coupling thus enables a readout of the molecule's magnetic properties with the electronic current but also leads to a strong back-action on the molecule's magnetic core.[1]

A less invasive approach consists of coupling the SMM to a second nonmagnetic

* Address correspondence to wolfgang.wernsdorfer@grenoble.cnrs.fr.

Received for review April 30, 2013 and accepted June 26, 2013.

Published online June 26, 2013
10.1021/nn402968k

molecular conductor, which is subsequently used as detector.[1] For such an indirect coupling, the magnetic core of the molecule is only weakly coupled to the conductor but can still affect its transport properties, thus enabling an electronic readout with only minimal back-action.

Among the different possible detectors (nanowires, carbon nanotubes, quantum dots, molecules), the carbon nanotube stands out due to its unique structural, mechanical, and electronic properties.[1] Several designs of supramolecular quantum spintronic devices have been recently proposed, where a carbon nanotube is used to probe individual molecular spins *via* different coupling mechanisms (magnetic flux, electronic, or mechanical).[1]

One can for instance probe the magnetic flux emanating from a single-molecule magnet grafted onto a SQUID magnetometer based on carbon nanotubes.[15,16] With the cross section of a carbon nanotube (on the order of 1 nm^2) being comparable with the size of the molecular magnet, one would obtain an almost ideal flux coupling in a carbon nanotube SQUID and a flux sensitivity of $S_\Phi \approx 10^{-5}\ \Phi_0/(\mathrm{Hz})^{1/2}$.[15] Such a sensitivity would allow one to probe the magnetic flux generated by individual SMMs like lanthanide complexes $LnPc_2$,[3,17] which was estimated to be on the order of $\Phi_{SMM} \approx 10^{-4}\ \Phi_0$.[15,17]

Alternatively, one can couple a SMM to a state-of-the-art carbon nanotube transistor and use the electric current in the nanotube to probe and manipulate the spin of the SMM.[18,19] A carbon nanotube behaves as a quantum dot at very low temperatures, showing an impressive array of electronic properties ranging from Coulomb blockade[20] to Kondo effect.[21] In this regime, a carbon nanotube is sensitive to very small charge fluctuations in its environment, which results in a modulation of the conductance in the carbon nanotube quantum dot. For instance, the nanotube's conductance can be altered by the magnetization reversal of a SMM grafted to the carbon nanotube's sidewall, which gives rise to a supramolecular spin valve behavior.[18,19]

In this paper, we will demonstrate how to couple a SMM to a carbon nanotube nanoelectromechanical system (NEMS) and probe the molecular nanomagnet with the carbon nanotube's mechanical motion at cryogenic temperatures. We will describe the detection principle and the sensitivity of such a torque magnetometer. Furthermore, we will provide an overview on the fingerprint-like characteristics of a pristine carbon nanotube NEMS. In particular, we will address the modulation of the resonance frequency and the nonlinearity induced by an electric and magnetic field. Then, we describe fingerprint-like properties of a terbium double-decker SMM (hereafter $TbPc_2$) and provide a highly efficient grafting process of $TbPc_2$ SMMs onto a carbon nanotube NEMS. We will demonstrate that this grafting process conserves both the magnetic properties of the $TbPc_2$ and the mechanical properties

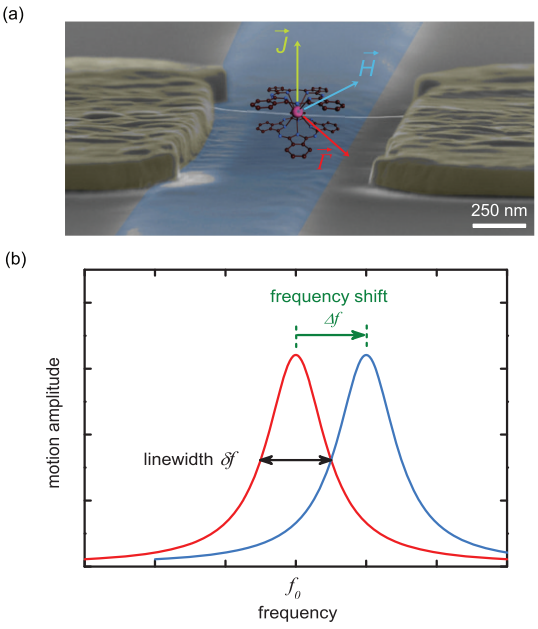

Figure 1. Carbon nanotube NEMS as magnetometer for molecular magnets. (a) False color SEM image of a carbon nanotube NEMS with a local metallic backgate (blue) functionalized with a molecular magnet (shown as a chemical structure overlaid on the image). Under the influence of a magnetic field $\vec{H}$ (blue arrow), the molecular magnet yielding a magnetic moment $\vec{J}$ (green arrow) will experience a magnetic torque $\vec{\Gamma}$ (red arrow), given by eq 1. By changing the magnetic field $|\vec{H}|$, one can therefore induce a change in the molecule's magnetic torque $|\vec{\Gamma}|$. If the molecular magnet is rigidly grafted to the carbon nanotube NEMS, a change of the torque $\Delta|\vec{\Gamma}|$ will induce an additional tension in the carbon nanotube beam, resulting in a shift of its resonance frequency $f_0 \rightarrow f_0 + \Delta f$. (b) Shift of the carbon nanotube NEMS' resonance frequency by the molecule's magnetic torque.

of the carbon nanotube. Finally, we will show that the mechanical bistability of a carbon nanotube NEMS in a nonlinear regime can be used to probe the magnetization reversal of a single $TbPc_2$ SMM grafted to the carbon nanotube.

RESULTS AND DISCUSSION

Carbon Nanotube NEMS as Magnetometer for Single-Molecule Magnets. We consider a SMM with a magnetic moment $\vec{\mu} = (g\mu_B/\hbar)\vec{J}$ to be rigidly grafted to the suspended carbon nanotube beam (Figure 1a).[22] Upon applying an external magnetic field $\mu_0\vec{H}_{ext}$, the SMM magnetization will experience a torque given by

$$\vec{\Gamma}_{SMM} = \mu_0\vec{\mu} \times \vec{H}_{ext} = \frac{g\mu_0\mu_B}{\hbar}\vec{J} \times \vec{H}_{ext} \qquad (1)$$

resulting in its rotation toward the magnetic field direction. In order to minimize the magnetic anisotropy energy the SMM starts to rotate, hence inducing mechanical strain in the suspended carbon nanotube beam.[22] The additional tension in the resonator will result in a shift of the mechanical resonance frequency of the carbon nanotube (Figure 1b).

Lassagne *et al.* studied the mechanical response of a carbon nanotube NEMS to the magnetization

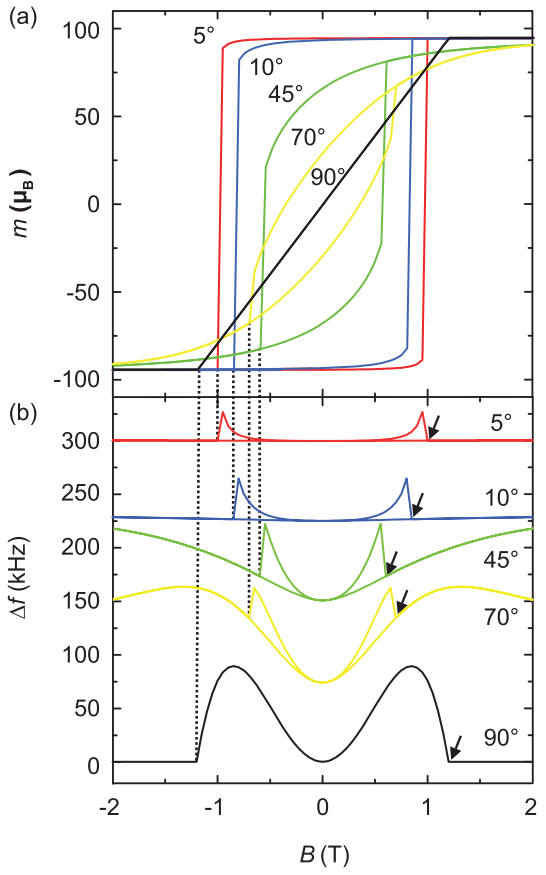

Figure 2. Mechanical response of a carbon nanotube NEMS to the magnetization reversal of a nanomagnet with uniaxial anisotropy. (a) Magnetic hysteresis loop of the nanomagnet for five different orientations of the magnetic field, with respect to its easy axis of magnetization θ_0 = 90, 70, 45, 10, 5°. One can observe the uniaxial anisotropy upon rotating the magnetic field away from the easy axis. (b) Frequency shift Δf as a function of the magnetic field. The curves translate the hysteretic behavior and the magnetic anisotropy of the nanomagnet. Modified from ref 22.

dynamics of a nanomagnet with a uniaxial magnetic anisotropy and a magnetic moment of 100 μ_B.[22] They determined the magnetic hysteresis of the nanomagnet (Stoner–Wolfahrt model, Figure 2a) and the magnetic field dependence of the carbon nanotube NEMS resonance frequency (Euler–Bernoulli formalism, Figure 2b) for different orientation of the magnetic field with respect to the nanomagnets easy axis. The model can be readily extended to a SMM, with a magnetic moment of a few μ_B.

The calculations reveal a discontinuous jump in the nanotube's resonance frequency, induced by the magnetization reversal of the nanomagnet (highlighted by the black arrows in Figure 2b). Furthermore, the field dependence of the resonance frequency translates the hysteretic behavior of the nanomagnet as well as its magnetic anistropy. For a magnetic field aligned close the nanomagnet's easy axis, a large hysteresis in the magnetization m and the frequency Δf is visible (θ_0 = 5°, red loop in Figure 2a,b). The hysteresis gradually disappears upon rotating the magnetic field into the hard plane of the molecule (θ_0 = 90°, black loop in Figure 2a,b). The maximum frequency shift reaches 90 kHz for a magnetic moment of 100 μ_B.

The sensitivity for such a magnetic torque detector is limited by the frequency noise induced by thermomechanical fluctuations and yields

$$\delta f_{th} = \frac{1}{2\pi}\left(\frac{k_B T}{k x_0^2}\frac{2\pi f_0 f_{BW}}{Q}\right)^{1/2} \quad (2)$$

For a resonance frequency f_0 = 50 MHz and quality factor $Q = 10^5$,[22,23] a spring constant $k \approx 10^{-4}$ N/m of the carbon nanotube NEMS,[22] one obtains a sensitivity of δf_{th} = 150 Hz/(Hz)$^{1/2}$ at 40 mK.

Furthermore, the carbon nanotube NEMS should provide a strong coupling with an individual molecular magnet in order to achieve the maximum sensitivity δf_{th}. Indeed, previous experiments on SMM grafted to a carbon nanotube NEMS revealed a strong coupling on the order of 1 MHz between an individual molecular spin and the nanotube's mechanical motion.[24]

One should therefore be able to reach a sensitivity of 1 μ_B at cryogenic temperatures with such a carbon-based torque magnetometer, thus providing a mechanical readout scheme for a single (molecular) spin.

Alternatively, one could also use the nonlinearity of the carbon nanotube NEMS developing at higher drive powers as a detector for the reversal of a molecular spin. Indeed, a characteristic bistable state develops for the mechanical motion in the nonlinear regime, and one observes an asymmetric resonance line shape with hysteresis between upward and downward frequency sweeps. In this bistable region, the carbon nanotube NEMS is unstable and a perturbation of the mechanical motion can result in a transition between the two metastable states, causing a jump in the nanotube's conductance (Figure 3). Due to the strong nonlinearity in carbon nanotube NEMS,[23,25,26] the detector signal associated with this transition yields a high signal-to-noise ratio. Furthermore, the nonlinearity can be tuned by electric fields *via* the gate and bias voltages,[25] which provides an electrical control over the mechanical bistability and thus over the magnitude of the detector signal. The mechanical bistability in a carbon nanotube NEMS can be used to probe a single molecular spin, as we will demonstrate in the following article.

Pristine High-*Q* Carbon Nanotube NEMS. At cryogenic temperatures, a carbon nanotube NEMS is in a regime of Coulomb blockade, and the electronic transport is governed by single-electron tunneling (SET).[20] It has been demonstrated in recent experiments that the nanotube's mechanical motion affects the electron transport in the carbon nanotube NEMS, thus enabling an electronic/current readout for nanomechanical oscillations in this system.[25,26]

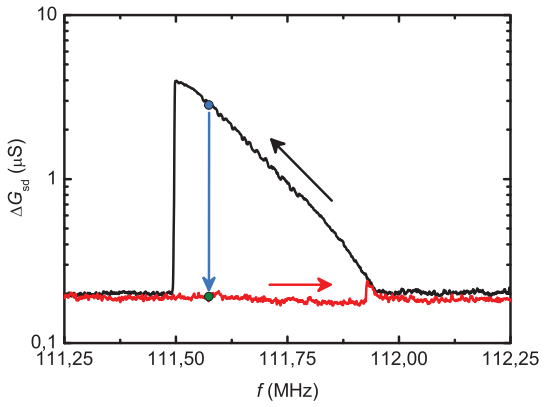

Figure 3. Nonlinear detection scheme for SMM magnetization reversal. In this bistable state, an asymmetric line shape develops with a hysteresis between up- and downward frequency sweeps (red and black curves, respectively). In the bistable region, the change of tension induced by the magnetization reversal of a SMM on the carbon nanotube (see text) can result in a switching from the upper (blue dot) to the lower branch (green dot) of the resonance line shape, causing a jump in the nanotube's conductance.

On the other hand, SET in a carbon nanotube NEMS can also be considered as an external perturbation to the nanotube's mechanical motion. This perturbation can be described as an electrodynamic force acting on the carbon nanotube. The contribution of this force, which is in phase with the mechanical motion, is responsible for a frequency modulation Δf, whereas a contribution of the force which is out of phase with mechanical motion induces a modification of the dissipation and the quality factor Q.[23,25,27]

Based on previous observations,[23,25−28] we will demonstrate in the following that the mechanical response of a carbon nanotube NEMS to SET can be controlled by both electric fields (*via* gate voltage) and magnetic fields, providing us with a fingerprint of a nanotube's mechanical motion at cryogenic temperatures (Figure 4).

Mechanical Fingerprint: SET Modulation of Frequency and Nonlinearity by Gate Voltage. It has been demonstrated in previous measurements that the mechanical response of a carbon nanotube NEMS to SET can be controlled by electric fields (*i.e.*, *via* gate and bias voltages).[23,25−27]

In a linear driving regime of the carbon nanotube NEMS (device #1, $P_{RF} = -90$ dBm), we observe indeed a characteristic frequency softening induced by single-electron fluctuations (and the current) when tuning the gate voltage through a Coulomb peak (Figure 5a). As expected for low driving power, the resonator also behaves as a harmonic oscillator and exhibits a Lorentzian line shape with a quality factor of $Q = 10^5$ (Figure 5b).

Upon increasing the drive amplitude ($P_{RF} = -70$ dBm), the carbon nanotube NEMS is evolving from a harmonic oscillator to a Duffing-like oscillator. In this case, we observe the characteristic asymmetric line shape associated with a nonlinear driving regime (Figure 5d).

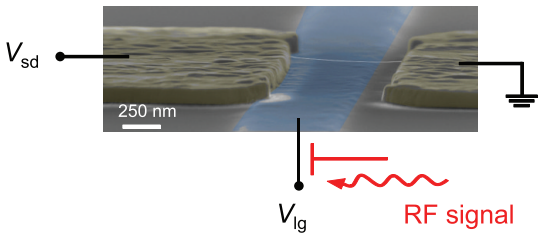

Figure 4. Pristine high-*Q* carbon nanotube NEMS. False color SEM image of a suspended carbon nanotube with a local metallic backgate (blue) and nanotube length of 850 nm. The RF actuation signal is injected into the local metallic gate through a home-built bias *T*. As the induced mechanical motion changes the charge flow through the CNT quantum dot and *vice versa*, we can detect the CNT resonance through a change in zero bias conductance.

In addition, SET in the carbon nanotube also modifies the line shape of the resonance feature (Figure 5c). This modulation of the nonlinearity by single-electron fluctuations (and the current) is consistent with previous observations.[25,26]

Mechanical Fingerprint: SET Modulation of Frequency and Nonlinearity by Magnetic Fields. A magnetic field applied along the carbon nanotube's axis shifts the chemical potential landscape in the carbon nanotube quantum dot.[29−31] A magnetic field H_x applied parallel to the nanotube therefore modulates the conductance dI_{sd}/dV_{sd} or SET in the carbon nanotube quantum dot as depicted in Figure 6. Additionally, the magnetic field can also modulate the tunnel barriers and the tunnel couplings $\Gamma_{s,d}$ at the interface between the carbon nanotube and the metal leads.[28] The effect is attributed to an increased band gap in the carbon nanotube at higher magnetic fields.[28]

A change in the conductance dI_{sd}/dV_{sd} and/or the tunnel rates $\Gamma_{s,d}$ induced by magnetic fields (and electric fields) furthermore modulates the carbon nanotube's resonance frequency and dissipation, as demonstrated in previous experiments.[23,28] Indeed, we observe a shift of the nanotube's frequency f_0 in device #1 at low driving power when tuning the magnetic field (indicated by the dashed line in Figure 6a). For larger driving power, the change in conductance induced by the magnetic field is associated with a strong modulation of the resonance line shape and nonlinearity (Figure 6).

Carbon Nanotube NEMS Functionnalized with Single-Molecule Magnets. In this section, we will present the fingerprint-like characteristics for a particular SMM, a bis(phthalocyaninato)terbium(III) molecule. We will describe a grafting procedure of this SMM onto a carbon nanotube NEMS and demonstrate that both the SMM's magnetic fingerprint and the NEMS mechanical fingerprint are conserved. Finally, we present evidence for a magnetization reversal in a $TbPc_2$ SMM induced by the carbon nanotube mechanical motion.

$TbPc_2$ Single-Molecule Magnet. The $TbPc_2$ is a rare earth SMM in which the magnetic moment is carried by a

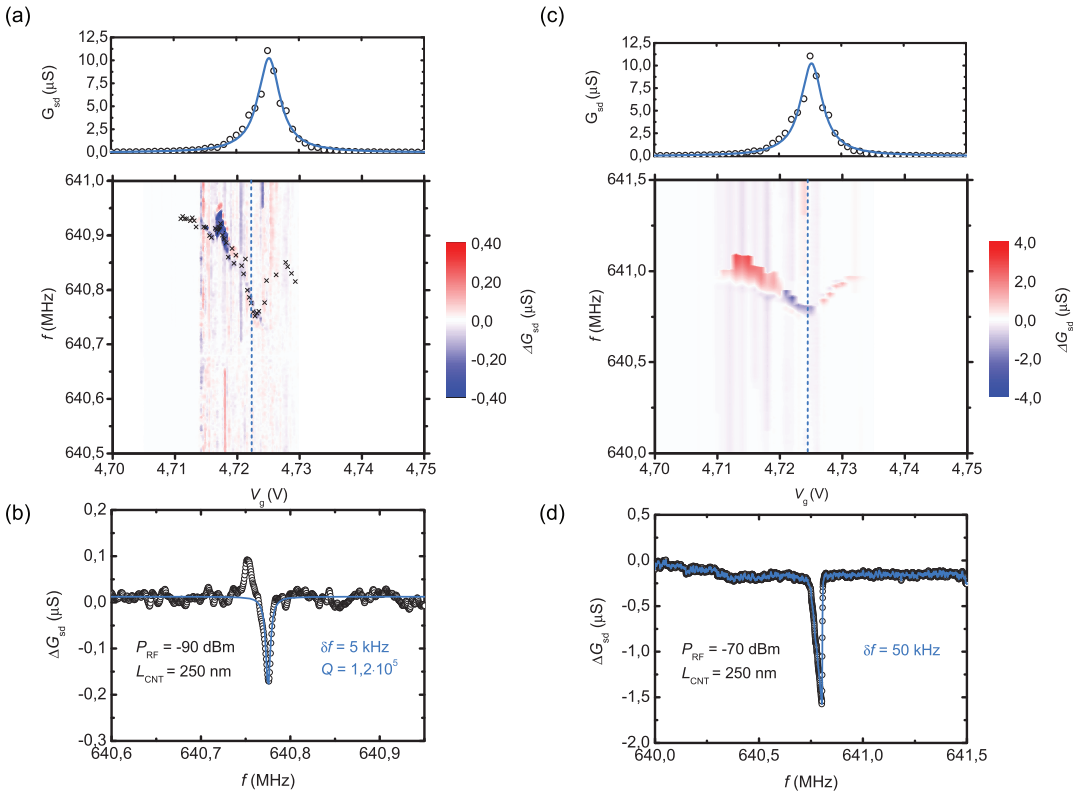

Figure 5. Gate dependence of the resonance frequency and nonlinearity in a pristine carbon nanotube NEMS (device #1). The device length was estimated to 250 nm. Linear driving regime ($P_{RF} = -90$ dBm): (a) conductance G_{sd} of the carbon nanotube NEMS as a function of the gate voltage V_g (top panel); conductance change $\Delta G_{sd} = G_{sd}(f) - G_{sd}(f = 0)$ induced by the mechanical motion as function of the RF drive frequency f and the gate voltage V_g (bottom panel). The black crosses highlight the mechanical resonance frequency f_0 of the NEMS. (b) Conductance ΔG_{sd} as a function RF drive frequency f at a gate voltage of $V_g = 4.725$ V, as denoted by the dashed blue line in (a). The resonance line width $\delta f = 5$ kHz leads to a quality factor of $Q = 120\,000$. The solid blue line is a Lorentzian fit of the resonance frequency. Nonlinear driving regime ($P_{RF} = -70$ dBm): (c) conductance G_{sd} of the carbon nanotube NEMS as a function of the gate voltage V_g (top panel); conductance change $\Delta G_{sd} = G_{sd}(f) - G_{sd}(f = 0)$ induced by the mechanical motion as function of the applied RF frequency f and the gate voltage V_g (bottom panel). (d) Conductance ΔG_{sd} as a function RF drive frequency f at a gate voltage of $V_g = 4.725$ V, as denoted by the dashed blue line in (c). The solid blue line is to guide the eye. All measurements are performed at a temperature of $T = 20$ mK.

single Tb^{3+} ion sandwiched between two organic phthalocyanine (Pc) ligand planes.[17,24] The $TbPc_2$ has a $S = 1/2$ radical delocalized over the Pc ligand planes. Due to $\pi-\pi$ interaction, this radical can easily hybridize with the π-electrons of any form of sp^2-carbon without affecting the magnetic properties of the Tb^{3+} ion.[4,5,17,24] The pyrene arm and the six hexyl groups added to one of the Pc planes are known for an attractive van der Waals interaction with sp^2-carbon and further enhance the grafting efficiency.[4,18,19] Moreover, the hexyl groups induce a steric hindrance in the molecule which prevents the reaggregation of the $TbPc_2$ in a solution and the formation of $TbPc_2$ clusters on the sidewall of the carbon nanotube.[18,19]

The highly anisotropic 4f shell of the Tb^{3+} ion and its intrinsically strong spin−orbit coupling results in a magnetic ground state of $J = 6$ and a pronounced uniaxial magnetic anisotropy (Figure 7a). The ground state doublet $J_z = \pm 6$ is separated from the excited states by several hundreds of Kelvin, which makes the $TbPc_2$ an Ising-like spin system at low temperature ($T < 5$ K) and small magnetic field ($B < 10$ T).[17,24] A strong hyperfine interaction with the nuclear spin $I = 3/2$ of the Tb^{3+} ion splits the ground state doublet $J_z = \pm 6$ into four states each (Figure 7b). Finally, the ligand field generates a small transverse magnetic anisotropy resulting in avoided level crossings (black circles in Figure 7b).[17,24]

At cryogenic temperatures, magnetization reversal can occur through two different processes. Around zero magnetic field, the avoided level crossings allow for quantum tunneling of magnetization $|J_z,I_z\rangle \rightarrow |-J_z,I_z\rangle$.[17−19] At high magnetic fields, the magnetization reverses through a direct relaxation process involving noncoherent tunneling events combined with the emission of a phonon (Figure 7b).[24]

Electronic Readout of the Magnetization Reversal in a $TbPc_2$ Grafted to a Carbon Nanotube NEMS. The study of the magnetization reversal of the $TbPc_2$ molecules grafted to the carbon nanotube NEMS are carried out in a $^3He/^4He$ dilution refrigerator with a base temperature of 20 mK using an electronic readout (Figure 8). It has been demonstrated by Urdampilleta *et al.*[18,19] that the magnetization reversal of a $TbPc_2$ SMM affects

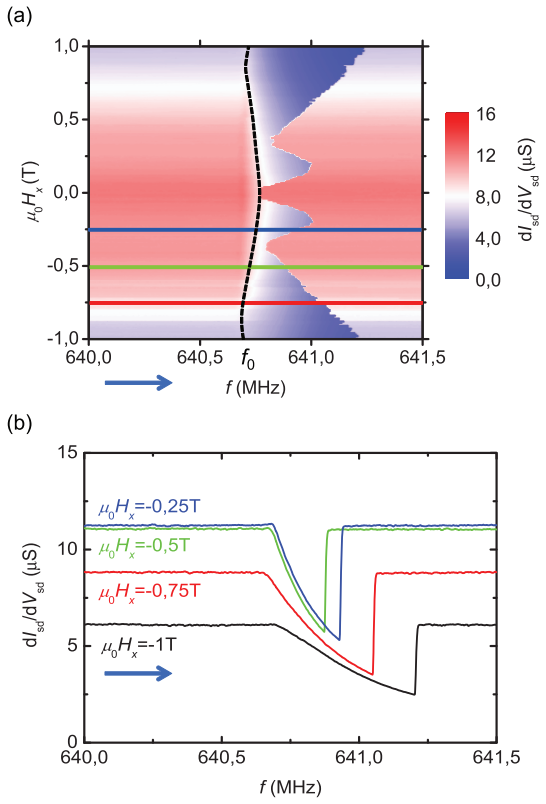

Figure 6. Magnetic field dependence of the resonance frequency and nonlinearity in a pristine carbon nanotube NEMS (device #1). (a) Differential conductance of the carbon nanotube NEMS as a function of the applied RF frequency f and the magnetic field component H_x parallel to the carbon nanotube axis. The measurement is performed in a nonlinear driving regime of the NEMS ($P_{RF} = -70$ dBm) at a gate voltage $V_{lg} = 4.725$ V and a temperature of $T = 20$ mK. The RF frequency is swept toward larger frequencies with 5 kHz/s (blue arrow) and the magnetic field is incremented in steps of 1 mT. The dashed black line corresponds to the modulation of resonance frequency f_0 in a linear driving regime ($P_{RF} = -90$ dBm). (b) Conductance G_{sd} as a function RF drive frequency f at four values of magnetic field as highlighted by the horizontal lines in (a). The blue arrow denotes the frequency sweep direction.

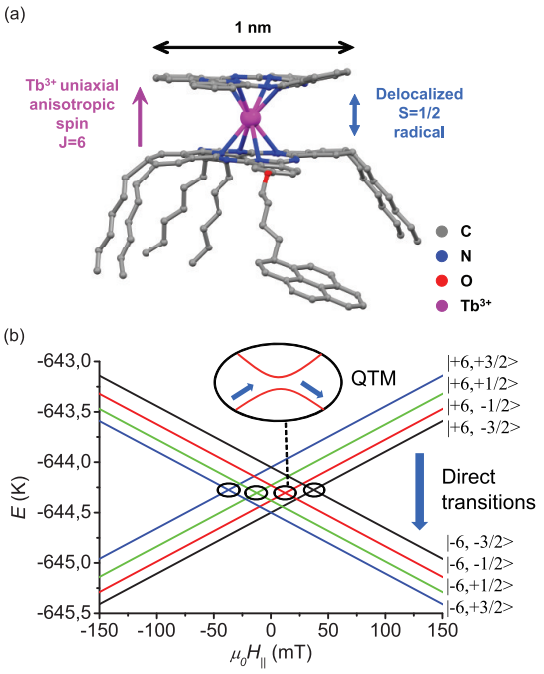

Figure 7. $TbPc_2$ SMM. (a) Schematic representation of a pyren-substituted $TbPc_2$ SMM. A Tb^{3+} ion (pink) is sandwiched between two organic phthalocyanine (Pc) ligand planes. The high anisotropy of the 4f shell in the Tb^{3+} ion and the strong spin−orbit coupling results in a magnetic ground state $J = 6$ with $J_z = \pm 6$. The SMM also yields a spin $S = 1/2$ radical delocalized over the Pc planes, which can hybridize with the π-electrons of carbon nanotubes *via* $\pi-\pi$ interaction. A pyrene arm and six hexyl groups further enhance the grafting efficiency to carbon nanotubes. (b) Zeeman diagram of the ground state doublet $J_z = \pm 6$. A strong hyperfine interaction splits the ground state doublet into the four nuclear spin states of the Tb^{3+} ion. The magnetization reversal of the $TbPc_2$ SMM can occur *via* quantum tunneling of magnetization (QTM) at the four avoided level crossings around zero field (highlighted by the black circle) or *via* direct transition involving the emission of a phonon.

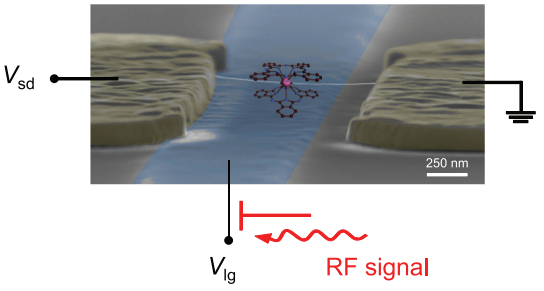

Figure 8. Carbon nanotube NEMS functionnalized with $TbPc_2$ SMM's. False color SEM image of a suspended carbon nanotube with a local metallic backgate (blue) functionalized with a $TbPc_2$ SMM (shown as a chemical structure overlaid on the image).

the electronic transport in a (suspended) carbon nanotube quantum dot at cryogenic temperatures, giving rise to a characteristic supramolecular spin valve behavior (Figure 9).

They demonstrated that two SMMs, coupled to the carbon nanotube *via* $\pi-\pi$ interaction, act as spin polarizer and analyzer for the conduction electrons in the carbon nanotube channel. Mediated by exchange interaction, the magnetic moment of each molecule induces a localized spin-polarized dot in the carbon nanotube quantum dot, which can be controlled by a magnetic field (Figure 9b,c).

At large negative magnetic fields, both molecular spins are oriented in parallel to each other and the quantum dot is in a high conductance state. Upon increasing the magnetic field (following the red trace in Figure 9a), the molecular spin A is reversed by quantum tunneling of magnetization close to zero field, resulting in an antiparallel spin orientation and a current blockade in the quantum dot (Figure 9b). By further increasing the field, the second spin B is reversed by a direct transition, restoring a parallel spin orientation and the high conductance regime in the quantum dot (Figure 9c). After reversing the sweep

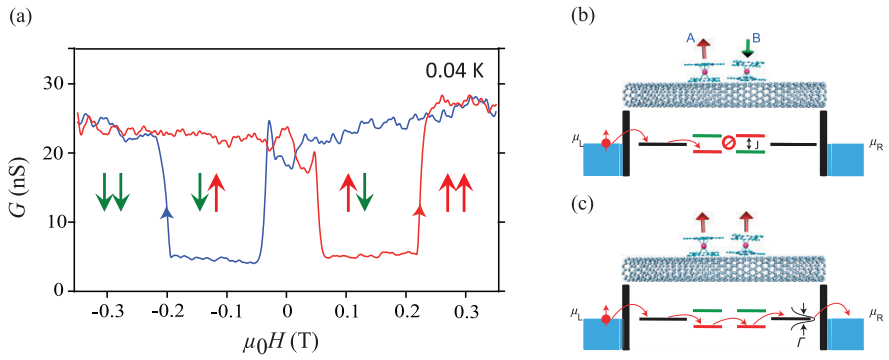

Figure 9. Spin valve behavior in a supramolecular spintronic device based on a carbon nanotube quantum dot functionnalized with $TbPc_2$ SMMs. Figures from refs 18 and 19. (a) Butterfly hystersis loop at $T = 40$ mK. (b) Antiparallel spin configuration. The spin states are inversed in the dot A, and the energy mismatch between levels with identical spin results in a current blockade. (c) Parallel spin configuration for both molecules A and B. Energy levels with the same spin are aligned, allowing electron transport through the carbon nanotube.

direction, one obtains the characteristic butterfly hysteresis loop of a spin valve device with a magnetoresistance ratio $(G_P - G_{AP})/G_{AP}$ up to 300%. A detailed description of the mechanism can be found in refs 18 and 19. Each current switching event, or switching field, can be attributed to the magnetization reversal of a SMM, thus providing us with an electronic readout scheme for a molecular spin.

Conservation of the Molecule's Magnetic Fingerprint. It was previously demonstrated that the van der Waals interaction between the $TbPc_2$ Pc ligand planes and the sidewall of the carbon nanotube leaves the magnetism of the Tb^{3+} ion intact.[4,18,19] It was also shown that the magnetic anisotropy of the above-described spin valve effect is in very good agreement with the uniaxial anisotropy of the Tb^{3+} spin and therefore provides a magnetic fingerprint for the $TbPc_2$ SMM.[18,19]

We observe this magnetic fingerprint on 100% of the carbon nanotube devices after grafting, indicating a highly efficient grafting process which conserves the magnetic properties of Tb^{3+} ion as demonstrated in previous works.[4,18,19] We performed upward (trace) and downward (retrace) magnetic field sweeps at different field orientations in the plane of the sample. Figure 10 depicts the difference in conductance between trace and retrace, that is, the magnetic hysteresis as a function of the in-plane magnetic field angle for two $TbPc_2$ concentrations. At high $TbPc_2$ concentration of 5×10^{-6} mol/L, one observes at least two easy axis of magnetization corresponding to two $TbPc_2$ SMMs with different orientations (Figure 10a). One can subsequently reduce the $TbPc_2$ concentration until two molecules remain and then study the magnetization reversal attributed to one of those $TbPc_2$ molecules (Figure 10b).

Conservation of the Carbon Nanotube's Mechanical Fingerprint. The mechanical motion of the carbon nanotube resonator is characterized as described above. For a concentration of $TbPc_2$ of 10^{-7} mol/L in solution, we observe a mechanical resonance with a frequency

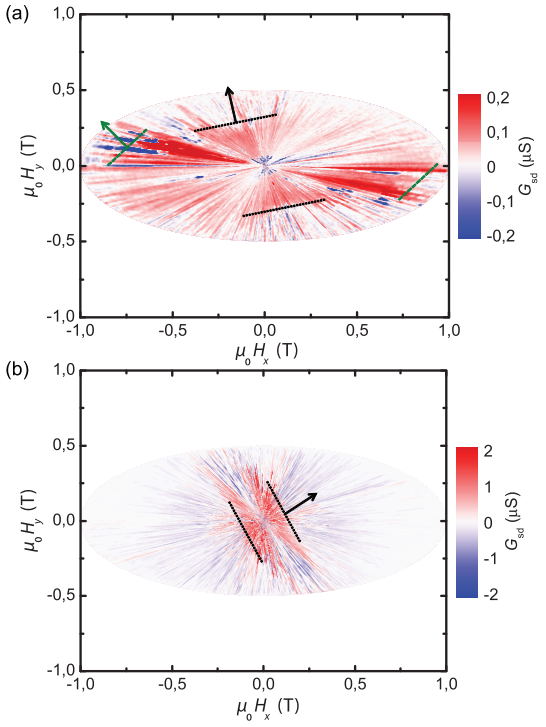

Figure 10. Magnetic fingerprint for $TbPc_2$ SMM for concentrations in solution of (a) 5×10^{-6} mol/L and (b) 5×10^{-7} mol/L. The arrows depict to the easy axis of the respective molecule, whereas the dashed lines indicate the corresponding switching fields. The white color code indicates a region of zero magnetic hysteresis, whereas the blue or red color code corresponds to a bistable region.

around 100 MHz (Figure 11a) and a quality factors on the order of $Q \sim 18\,000$ for low drive power $P_{RF} = -100$ dBm (Figure 11b). At larger driving power, $P_{RF} = -90$ dBm, we observe a characteristic Duffing nonlinearity in the carbon nanotube NEMS (Figure 11c,d). Both the nonlinearity and the resonance frequency modulate with the gate voltage (*i.e.*, the current or SET in the device).

The observed quality factor at low driving power is at least an order of magnitude smaller than for the ultraclean carbon nanotube NEMS described earlier

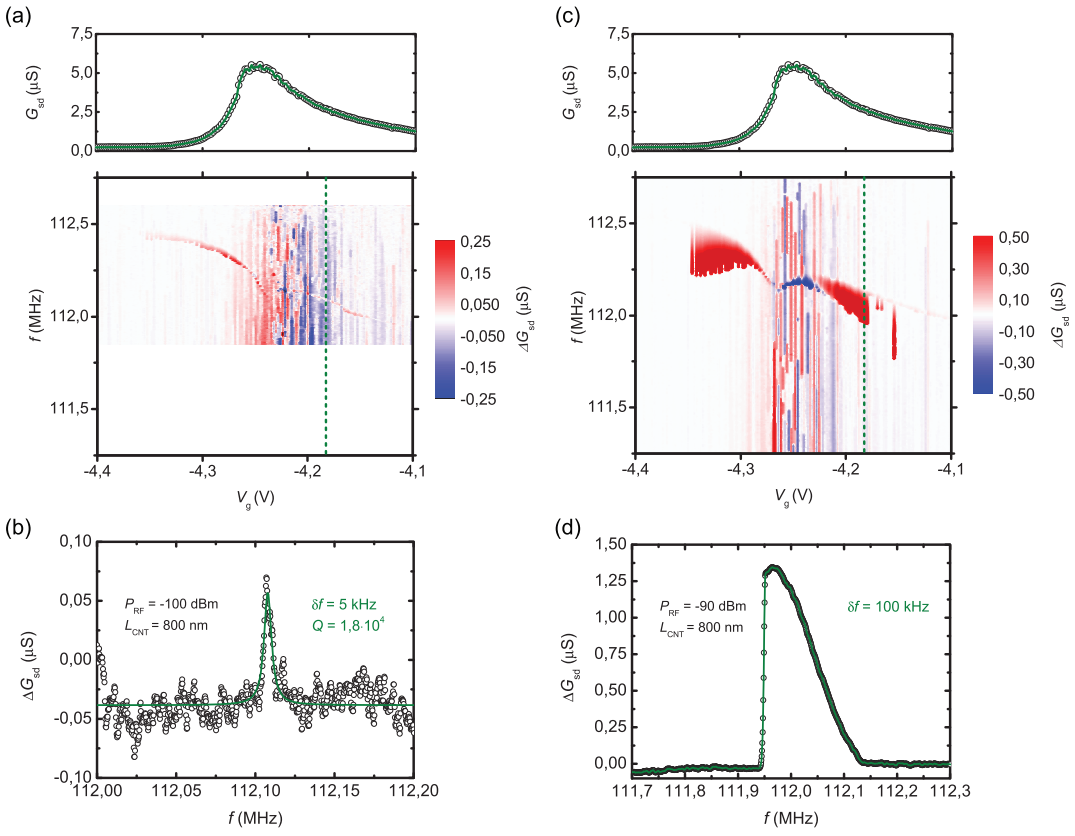

Figure 11. SET dependence of the resonance frequency and nonlinearity in a carbon nanotube NEMS functionalized with $TbPc_2$ SMM's (device #2). Linear driving regime ($P_{RF} = -100$ dBm): (a) conductance G_{sd} of the carbon nanotube NEMS as a function of the gate voltage V_g (top panel) and change in conductance ΔG_{sd} as function of the RF drive frequency f and the gate voltage V_g (bottom panel). (b) Change in conductance ΔG_{sd} as a function RF drive frequency f at a gate voltage of $V_g = -4.18$ V, as denoted by the dashed green line in (a). The resonance line width $\delta f = 5$ kHz leads to a quality factor of $Q = 18\,000$. The lower resonance frequency and quality factor indicate an additional mass load, consistent with the presence of several $TbPc_2$ SMMs on the sidewall of the carbon nanotube. The solid green line is a Lorentzian fit of the resonance frequency. Nonlinear driving regime ($P_{RF} = -90$ dBm): (c) conductance G_{sd} of the carbon nanotube NEMS as a function of the gate voltage V_g (top panel) and change in conductance ΔG_{sd} as function of the applied RF frequency f and the gate voltage V_g (bottom panel). (d) Change in conductance ΔG_{sd} as a function RF drive frequency f at a gate voltage of $V_g = -4.18$ V, as denoted by the dashed green line in (c). The solid green line is to guide the eye. All measurements are performed at a temperature of $T = 20$ mK.

(see Figure 5). The result indicates that the grafted $TbPc_2$ molecules induce additional dampening to the mechanical motion of the nanotube. Indeed a $TbPc_2$ SMM grafted to the sidewall of a carbon nanotube can be considered as two-level system (TLS) and induce additional dissipation in the NEMS.[26,32] The additional $TbPc_2$ mass load also reduces the resonance frequency and therefore also the quality factor.

Increasing the $TbPc_2$ concentration in solution by at least an order of magnitude results in a higher density of grafted $TbPc_2$ on the carbon nanotube. This considerably increases the number of two-level systems as well as the mass load and therefore the dissipation. Indeed, no mechanical fingerprint of the carbon nanotube NEMS was detected for $TbPc_2$ concentrations in solution higher than 10^{-7} mol/L.

We can conclude that grafting $TbPc_2$ single-molecule magnets from low concentration $TbPc_2$ solution onto carbon nanotube NEMS conserves both the magnetic properties of the $TbPc_2$ and the mechanical properties of the resonator and is therefore a key component for the fabrication of carbon nanotube-based supramolecular spintronic device.

Magnetization Reversal Detection of a $TbPc_2$ by Nonlinear Mechanical Motion. Finally, we study the magnetization reversal of a $TbPc_2$ SMM grafted to a carbon nanotube NEMS (device #2, introduced in the previous section) *via* the nanotube's mechanical motion. For this purpose, we perform magnetic field sweeps along the nanotube's axis from positive to negative values (downward, Figure 12a,c) and back (upward, Figure 12b,d) at different values of the applied RF frequency, f, while monitoring the nanotube's conductance. The measurement is performed in a linear and nonlinear driving regime of the NEMS, at a gate voltage $V_{lg} = -4.1$ V and a temperature of $T = 20$ mK.

In the linear driving regime of the NEMS ($P_{RF} = -95$ dBm), we observe a significant modulation of the resonance frequency by a magnetic field (Figure 12a,b) in agreement with previous experiments.[28] We also observe a small hysteresis in the magnetoconductance, which is consistent with the magnetization reversal of

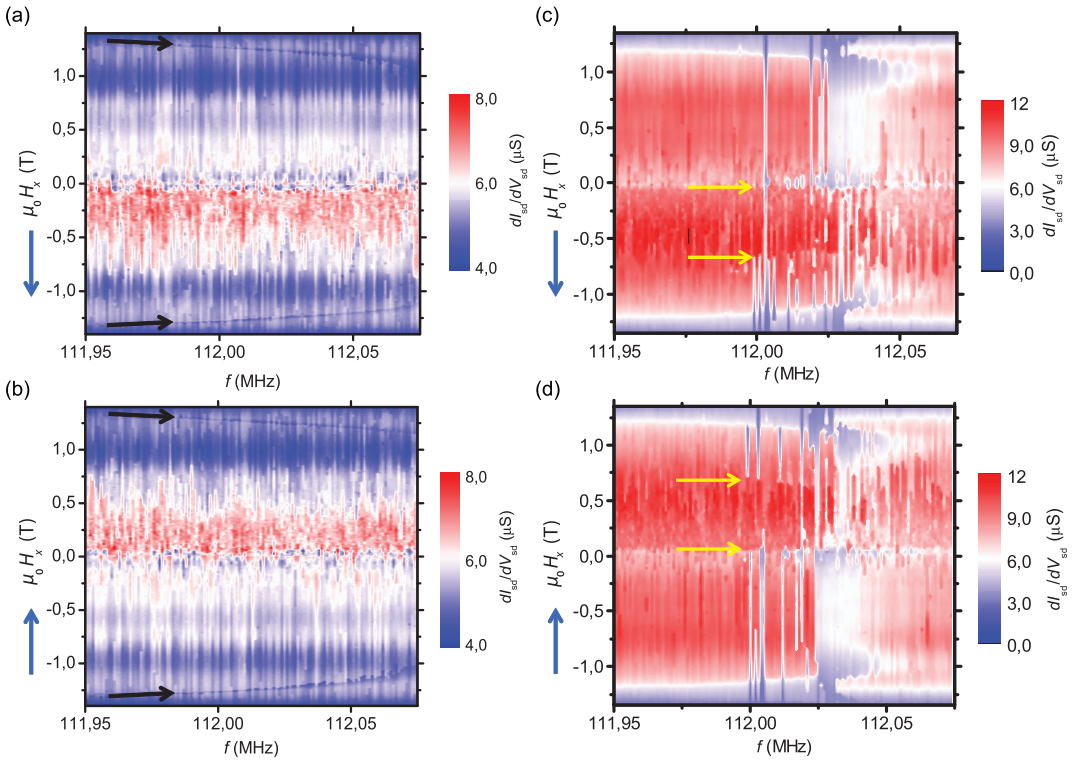

Figure 12. Magnetic field dependence of the resonance frequency in a carbon nanotube NEMS functionnalized with $TbPc_2$ SMM's (device #2). Linear driving regime (P_{RF} = −95 dBm): (a,b) differential conductance in the carbon nanotube NEMS as a function of the applied RF frequency f and the magnetic field component H_x parallel to the carbon nanotube axis. The magnetic field is swept (a) downward and then (b) upward with 100 mT/s, and the RF frequency f is incremented in steps of 1 kHz. The black arrows indicate the position of the resonance frequency. Nonlinear driving regime (P_{RF} = −80 dBm): (c,d) differential conductance in the carbon nanotube NEMS as a function of the applied RF frequency f and the magnetic field component H_x parallel to the carbon nanotube axis for (c) downward and (d) upward magnetic field sweeps. The yellow arrow in (c) and (d) indicates a jump in the differential conductance associated with the magnetization reversal of a single $TbPc_2$ SMM. The dashed lines represent the magnetic field modulation of the resonance frequency in the linear regime (P_{RF} = −95 dBm). All measurements are performed at a gate voltage V_{lg} = −4.10 V and a temperature of T = 20 mK.

paramagnetic centers in the carbon nanotube activated by the large magnetic field sweep rate. An identical magnetic hysteresis was recently reported in the magnetoconductance of graphene devices.[33]

At higher driving power (P_{RF} = −80 dBm), we find a change of the NEMS nonlinearity in a magnetic field H_x in agreement with the NEMS's frequency and nonlinearity response to SET induced by a magnetic field presented in ref 28. In addition to the modulation of the nonlinearity, we also observe abrupt jumps in the nanotube's conductance around $\mu_0 H_x = 0$ and −0.65 T for downward magnetic field sweeps (respectively $\mu_0 H_x$ = 0 and +0.65 T for upward magnetic field sweeps) and for RF frequencies between f = 112 MHz and f = 112.075 MHz. The conductance jumps are highlighted by the yellow arrows in Figure 12c,d.

For better visibility, the values of magnetic field corresponding to these conductance jumps, the switching fields $H_{x,SW}$, are extracted for down- and upward magnetic field sweeps and plotted as a function of the applied RF frequency f (Figure 13). The conductance switching either occurs around $\mu_0 H_x = 0$ or around ±0.65 T, with a hysteresis between up- and downward magnetic field sweeps (Figure 13). The

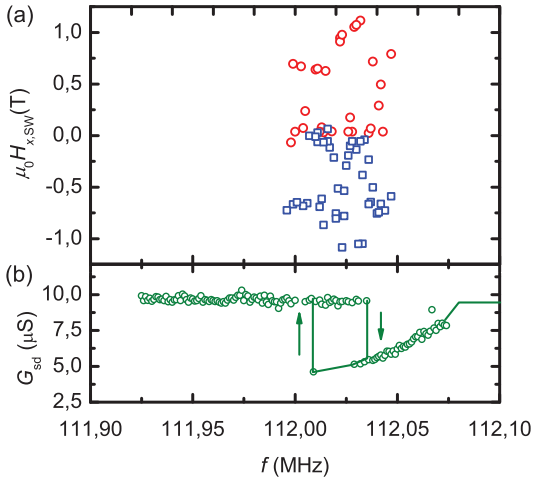

Figure 13. Magnetization reversal of a $TbPc_2$ SMM in device #2 as a function of RF frequency. (a) Switching fields $\mu_0 H_{x,SW}$ of the $TbPc_2$ SMM extracted from downward (blue open squares) and upward (red open dots) magnetic field sweeps in (c) and (d), respectively, as a function of the applied RF frequency f. The measurements are performed in a nonlinear driving regime of the NEMS (P_{RF} = −80 dBm) at a temperature of T = 20 mK and a magnetic field sweep rate of 100 mT/s. (b) Mechanical resonance line shape at a driving power of P_{RF} = −80 dBm and magnetic field of $\mu_0 H_x$ = 0.65 T. The solid green lines are a guide for the eye.

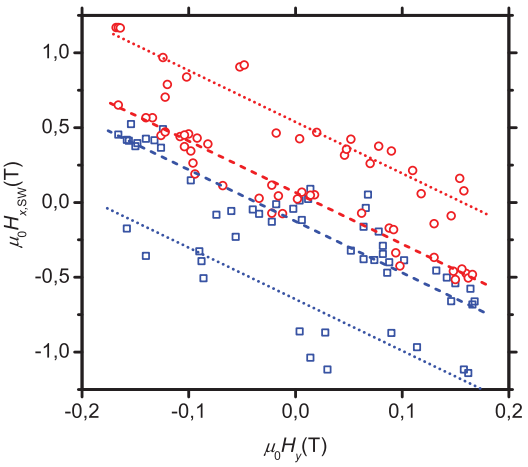

Figure 14. Magnetization reversal of a $TbPc_2$ SMM in device #2 at the nanotube's resonance frequency $f_0 = 112.025$ MHz as a function of the transverse magnetic field. Switching fields $\mu_0 H_{x,SW}$ of the $TbPc_2$ SMM for downward (blue open squares) and upward (red open dots) magnetic field sweeps as a function of the transverse magnetic field $\mu_0 H_y$. The measurements are performed in a nonlinear driving regime of the NEMS ($P_{RF} = -80$ dBm) at a temperature of $T = 20$ mK and a magnetic field sweep rate of 100 mT/s.

hysteretic and stochastic behavior of the conductance switching is characteristic for the magnetization reversal of a $TbPc_2$ SMM.[18,19] The switching events around zero field in Figure 13 could therefore be attributed to QTM events, whereas the switching events around $\mu_0 H_{x,SW} = \pm 0.65$ T correspond to a direct relaxation of the $TbPc_2$ SMM. Finally, the magnetization reversal of the $TbPc_2$ appears only in a strongly nonlinear driving regime (Figure 12) and is restricted to the bistable region at the resonance frequency (Figure 13).

Additionally, we study the switching fields $H_{x,SW}$ at a frequency $f = 112.025$ MHz (depicted by the light blue dashed line in Figure 13) as a function of a transverse magnetic field component H_y (Figure 14). For both downward and upward magnetic field sweeps (Figure 14), the switching fields strongly depend on the transverse field H_y and follow two parallel lines, as depicted by the dashed and dotted lines in Figure 14. The projection of these switching fields on an axis perdendicular to the dashed (dotted) lines is constant, which is also consistent with the uniaxial magnetic anisotropy of a single $TbPc_2$ SMM. The dashed and dotted lines in Figure 14 thus correspond to QTM events and direct transition events, respectively. Therefore, the conductance switching observed in Figure 13 and Figure 14 can indeed be attributed to the magnetization reversal of a single $TbPc_2$ SMM.

These findings suggest that the nonlinear dynamics in the carbon nanotube enable the detection of the $TbPc_2$ magnetization reversal. Indeed, a bistable state develops for the mechanical motion in the nonlinear driving regime, and one observes an asymmetric resonance line shape with hysteresis between upward and downward frequency sweeps (red and black curve, respectively, in Figure 3). In this bistable region, the carbon nanotube NEMS is unstable and any perturbation of the mechanical motion results in a transition between the two metastable states. This mechanical bistability can for instance be used to probe the magnetization reversal of the SMM.

As the magnetization reversal occurs in the SMM, the resulting change of torque induces a variation of tension in the carbon nanotube according to the mechanism described in ref 22. For a working point in the bistable region (blue dot on the black curve in Figure 3), the change of tension induced by the SMM's magnetization reversal on the nanotube can therefore trigger a switching from the upper to the lower resonance branch, causing an abrupt change in the nanotube's conductance (Figure 3). Such a detection mechanism is limited to the nonlinear driving regime and to the bistable region at the resonance frequency, which is supported by the experimental evidence in Figure 13 and Figure 14.

CONCLUSION

In this article, we described a grafting process of a tailored $TbPc_2$ SMM to a carbon nanotube NEMS, which conserves both the mechanical properties of a carbon nanotube NEMS (high quality factors, nonlinearities, SET modulation, *etc.*) as well as the magnetic properties of a $TbPc_2$ SMM (uniaxial magnetic anisotropy, QTM, *etc.*). The noninvasive nature of the grafting process subsequently allows for a study of the SMM's magnetization reversal *via* the influence on the nanotube's mechanical oscillation. We found evidence that the mechanical bistability of a carbon nanotube NEMS in a nonlinear regime can be used to probe the magnetization reversal of the $TbPc_2$. Our results provide the first experimental evidence for the detection of a single spin by a mechanical degree of freedom on a molecular level and the first implementation of a molecular magnetometer based on a carbon nanotube NEMS.

EXPERIMENTAL SECTION

The suspended carbon nanotube NEMS are grown *via* an ultraclean, bottom-up fabrication process.[23−25,34] For this purpose, a 1 μm wide metallic local gate is patterned by optical deep ultraviolet (DUV) lithography and subsequent e-beam evaporation of Mo (20 nm) on a degenerately p-doped silicon wafer with a 300 nm thick layer of thermal SiO_2. A layer of 100 nm of Al_2O_3 is then deposited by atomic layer deposition. Using optical DUV lithography and e-beam evaporation of Mo (20 nm) and Pt (160 nm), source-drain electrodes are aligned above the local gate. Suspended carbon nanotubes are finally grown by CVD at 800 °C from a CH_4 feedstock and Fe/Mo catalyst spots patterned on the source-drain electrodes next to the junction.[23,24]

In a second step, pyrene-substituted $TbPc_2$ SMMs are synthesized in powder form as reported in ref 4. The $TbPc_2$ powder was subsequently dissolved in a solution of dichloromethane and then drop-casted onto the sample. The droplet is dried in a supercritical point dryer to avoid the destruction of the suspended carbon nanotubes through capillarity effects.[24] We performed depositions of $TbPc_2$ molecules on carbon nanotube NEMS from solutions with $TbPc_2$ concentrations ranging from 10^{-7} to 5×10^{-6} mol/L.

The measurements are carried out in a $^3He/^4He$ dilution refrigerator with a base temperature of 20 mK. The NEMS actuation and detection scheme used in our experiments[23,24] is similar to the one used by Steele and co-workers.[25,26] The RF actuation signal is injected into the gate electrode *via* a home-built bias T. As the induced mechanical motion changes the charge flow through the CNT quantum dot and *vice versa*, we can detect the CNT resonance through a change in zero bias conductance.[23] For magnetic field measurements, the refrigerator was equipped with two orthogonal field coils, generating up to 1.4 and 0.5 T, respectively, in the plane of the sample, with a maximum sweep rate of 250 mT/s. All measurements were done under zero bias with a standard lock-in technique.[23,24]

Conflict of Interest: The authors declare no competing financial interest.

Acknowledgment. This work is partially supported by the ANR-PNANO project MolNanoSpin No. ANR-08-NANO-002 and ERC Advanced Grant MolNanoSpin No. 226558. M.G. acknowledges the financial support from the RTRA Nanosciences Foundation. Samples were fabricated in the NANOFAB facility of the Neel Institute. We thank F. Balestro, E. Bonet, T. Crozes, J.P. Cleuziou, E. Eyraud, T. Fournier, R. Haettel, C. Hoarau, D. Lepoittevin, V. Nguyen, V. Reita, S. Thiele, C. Thirion, M. Urdampilleta, and R. Vincent.

REFERENCES AND NOTES

1. Bogani, L.; Wernsdorfer, W. Molecular Spintronics Using Single-Molecule Magnets. *Nat. Mater.* **2008**, *7*, 179–183.
2. Gatteschi, D.; Sessoli, R.; Villain, J. *Molecular Nanomagnets*; Oxford University Press: New York, 2006.
3. Ishikawa, N.; Sugita, M.; Ishikawa, T.; Koshihara, S.-y.; Kaizu, Y. Mononuclear Lanthanide Complexes with a Long Magnetization Relaxation Time at High Temperatures? A New Category of Magnets at the Single-Molecular Level. *J. Phys. Chem. B* **2004**, *108*, 11265–11271.
4. Kyatskaya, S.; Galan-Mascaros, J.-R.; Bogani, L.; Hennrich, F.; Kappes, M.; Wernsdorfer, W.; Ruben, M. Anchoring of Rare-Earth-Based Single-Molecule Magnets on Single-Walled Carbon Nanotubes. *J. Am. Chem. Soc.* **2009**, *131*, 15143–15151.
5. Lopes, M.; Candini, A.; Urdampilleta, M.; Reserbat-Plantey, A.; Bellini, V.; Klyatskaya, S.; Marty, L.; Ruben, M.; Affronte, M.; Wernsdorfer, W.; *et al.* Surface-Enhanced Raman Signal for Terbium Single-Molecule Magnets Grafted on Graphene. *ACS Nano* **2010**, *4*, 7531–7537.
6. Friedman, J. R.; Sarachik, M. P.; Tejada, J.; Ziolo, R. Macroscopic Measurement of Resonant Magnetization Tunneling in High-Spin Molecules. *Phys. Rev. Lett.* **1996**, *76*, 3830–3833.
7. Thomas, L.; Lionti, F.; Ballou, R.; Gatteschi, D.; Sessoli, R.; Barbara, B. Macroscopic Quantum Tunnelling of Magnetization in A Single Crystal of Nanomagnets. *Nature* **1996**, *383*, 145–148.
8. Wernsdorfer, W.; Sessoli, R. Quantum Phase Interference and Parity Effects in Magnetic Molecular Clusters. *Science* **1999**, *284*, 133–135.
9. Otte, A. F.; Ternes, M.; von Bergmann, K.; Loth, S.; Brune, H.; Lutz, C. P.; Hirjibehedin, C. F.; Heinrich, A. J. The Role of Magnetic Anisotropy in the Kondo Effect. *Nat. Phys.* **2008**, *4*, 847–850.
10. Komeda, T.; Isshiki, H.; Liu, J.; Zhang, Y.; Lorente, N.; Katoh, K.; Breedlove, B. K.; Yamashita, M. Observation and Electric Current Control of a Local Spin in a Single-Molecule Magnet. *Nat. Commun.* **2011**, *2*, 217–222.
11. Fu, Y.-S.; Schwsbel, J.; Hla, S.-W.; Dilullo, A.; Hoffmann, G.; Klyatskaya, S.; Ruben, M.; Wiesendanger, R. Reversible Chiral Switching of Bis(phthalocyaninato) Terbium(III) on a Metal Surface. *Nano Lett.* **2012**, *12*, 3931–3935.
12. Schwoebel, J.; Fu, Y.-S.; Brede, J.; Dilullo, A.; Hoffmann, G.; Klyatskaya, S.; Ruben, M.; Wiesendanger, R. Real-Space Observation of Spin-Split Molecular Orbitals of Adsorbed Single-Molecule Magnets. *Nat. Commun.* **2012**, *3*, 953–957.
13. Heersche, H. B.; de Groot, Z.; Folk, J. A.; van der Zant, H. S. J.; Romeike, C.; Wegewijs, M. R.; Zobbi, L.; Barreca, D.; Tondello, E.; Cornia, A. Electron Transport through Single Mn_{12} Molecular Magnets. *Phys. Rev. Lett.* **2006**, *96*, 206801.
14. Vincent, R.; Klyatskaya, S.; Ruben, M.; Wernsdorfer, W.; Balestro, F. Electronic Readout of a Single Nuclear Spin in a Single Molecule Transistor. *Nature* **2012**, *488*, 357–360.
15. Cleuziou, J.; Wernsdorfer, W.; Bouchiat, V.; Ondarcuhu, T.; Montioux, M. Carbon Nanotube Superconducting Interference Device. *Nat. Nanotechnol.* **2006**, *1*, 53–56.
16. Maurand, R.; Meng, T.; Bonet, E.; Florens, S.; Marty, L.; Wernsdorfer, W. First-Order $0-\pi$ Quantum Phase Transition in the Kondo Regime of a Superconducting Carbon-Nanotube Quantum Dot. *Phys. Rev. X* **2012**, *2*, 011009.
17. Ishikawa, N.; Sugita, M.; Wernsdorfer, W. Quantum Tunneling of Magnetization in Lanthanide Single-Molecule Magnets: Bis(phthalocyaninato)terbium and Bis(phthalocyaninato)-dysprosium Anions. *Angew. Chem., Int. Ed.* **2005**, *44*, 2931–2935.
18. Urdampilleta, M.; Klyatskaya, S.; Cleuziou, J.-P.; Ruben, M.; Wernsdorfer, W. Supramolecular Spin Valves. *Nat. Mater.* **2011**, *10*, 502–506.
19. Urdampilleta, M.; Klyatskaya, S.; Ruben, M.; Wernsdorfer, W. Landau-Zener Tunneling of a Single Tb^{3+} Magnetic Moment allowing the Electronic Read-Out of a Nuclear Spin. *Phys. Rev. B* **2013**, *87*, 195412.
20. Charlier, J.-C.; Blase, X.; Roche, S. Electronic and Transport Properties of Nanotubes. *Rev. Mod. Phys.* **2007**, *79*, 677–732.
21. Nygård, J.; Cobden, D. H.; Lindelof, P. E. Kondo Physics in Carbon Nanotubes. *Nature* **2000**, *408*, 342–346.
22. Lassagne, B.; Ugnati, D.; Respaud, M. Ultrasensitive Magnetometers Based on Carbon-Nanotube Mechanical Resonators. *Phys. Rev. Lett.* **2011**, *107*, 130801.
23. Ganzhorn, M.; Wernsdorfer, W. Dynamics and Dissipation Induced by Single-Electron Tunneling in Carbon Nanotube Nanoelectromechanical Systems. *Phys. Rev. Lett.* **2012**, *108*, 175502.
24. Ganzhorn, M.; Klyatskaya, S.; Ruben, M.; Wernsdorfer, W. Strong Spin-Phonon Coupling between a Single Molecule Magnet and a Carbon Nanotube Nanoelectromechanical System. *Nat. Nanotechnol.* **2013**, *8*, 165–168.
25. Steele, G. A.; Hüttel, A. K.; Witkamp, B.; Poot, M.; Meerwaldt, H. B.; Kouwenhoven, L. P.; van der Zant, H. S. J. Strong Coupling between Single-Electron Tunneling and Nanomechanical Motion. *Science* **2009**, *325*, 1103–1107.
26. Hüttel, A. K.; Steele, G. A; Witkamp, B.; Poot, M.; Kouwenhoven, L. P.; van der Zant, H. S. J. Carbon Nanotubes as Ultrahigh Quality Factor Mechanical Resonators. *Nano Lett.* **2009**, *9*, 2547–2552.
27. Lassagne, B.; Tarakanov, Y.; Kinaret, J.; Garcia-Sanchez, D.; Bachtold, A. Coupling Mechanics to Charge Transport in Carbon Nanotube Mechanical Resonators. *Science* **2009**, *325*, 1107–1110.
28. Meerwaldt, H. B.; Labadze, G.; Schneider, B. H.; Taspinar, A.; Blanter, Y. M.; van der Zant, H. S. J.; Steele, G. A. Probing the Charge of a Quantum Dot with a Nanomechanical Resonator. *Phys. Rev. B* **2013**, *86*, 115454.
29. Deshpande, V. V.; Bockrath, M. The One-Dimensional Wigner Crystal in Carbon Nanotubes. *Nat. Phys.* **2008**, *4*, 314–318.
30. Cleuziou, J.-P.; Wernsdorfer, W.; Ondarcuhu, T.; Monthioux, M. Electrical Detection of Individual Magnetic Nanoparticles Encapsulated in Carbon Nanotubes. *ACS Nano* **2011**, *5*, 2348–2355.

31. Datta, S.; Marty, L.; Cleuziou, J. P.; Tilmaciu, C.; Soula, B.; Flahaut, E.; Wernsdorfer, W. Magneto-Coulomb Effect in Carbon Nanotube Quantum Dots Filled with Magnetic Nanoparticles. *Phys. Rev. Lett.* **2011**, *107*, 186804.
32. Seoanez, C.; Guinea, F.; Neto, A. H. C. Dissipation Due to Two-Level Systems in Nanomechanical Devices. *Europhys. Lett.* **2007**, *78*, 60002.
33. Candini, A.; Alvino, C.; Wernsdorfer, W.; Affronte, M. Hysteresis Loops of Magnetoconductance in Graphene Devices. *Phys. Rev. B* **2011**, *83*, 121401.
34. Cao, J.; Wang, Q.; Wang, D.; Dai, H. Suspended Carbon Nanotube Quantum Wires with Two Gates. *Small* **2005**, *1*, 138–141.